Power Electronics and Drives
Volume 11(46), 2026 DOI: 10.2478/pead-2026-0015

Short-Horizon Finite-State Voltage Control of Bidirectional DC–DC Converter with Non-Minimum Phase Dynamics

Research paper

Fatemeh Rezayof Tatari*, Grzegorz Iwanski

Faculty of Electrical Engineering, Warsaw University of Technology, Warsaw, Poland

Received: 04 February, 2026; Received in the revised form: 26 March, 2026; Accepted: 14 April, 2026

Abstract: Bidirectional DC–DC converters play a critical role in DC microgrids by enabling regulated voltage conversion and bidirectional power flow between energy sources, storage systems and loads. However, achieving fast and robust voltage regulation in such converters remains challenging due to non-minimum phase (NMP) dynamics, digital implementation delays and model uncertainty. In the literature, short-horizon finite-state voltage control strategies are presented as desired methods for controlling these converters. In this paper, a systematic comparison of recent short-horizon finite-state control strategies—including single-horizon finite-set model predictive control (FS-MPC), compensated bang-bang (BB) control and BB control with doubled sampling frequency (DSF-BB)—is first presented. Subsequently, a novel model-free bang-bang (MF-BB) control strategy is proposed. The proposed model-free approach eliminates reliance on an explicit system model by generating the desired inductor-current reference directly from measured current signals, while preserving short-horizon operation and low computational complexity. The performance of the proposed method is then compared with existing approaches through comprehensive simulation studies under non-minimum phase operation and digital implementation delays. Additional evaluations consider parameter variations and conduction-mode transitions. The simulation and experimental results demonstrate that the proposed MF-BB strategy achieves transient response, settling time and steady-state voltage regulation comparable to the model-based methods while eliminating dependence on converter parameter accuracy. These findings highlight the effectiveness and practical suitability of the proposed approach for digitally controlled bidirectional DC–DC converters in DC microgrid applications.

Keywords: *bang-bang control • bidirectional DC–DC converter • finite-set model predictive control • finite-state control • non-minimum phase dynamics*

1. Introduction

In recent years, rapid growth in the use of renewable energy sources, battery energy storage systems and DC loads has significantly accelerated the deployment of DC microgrids (Bizhani et al., 2025). Compared with conventional AC architectures, DC microgrids offer higher efficiency, simpler power conversion stages and the elimination of challenges related to synchronisation, reactive power flow and harmonic distortion (Al-Ismail, 2021; Patel et al., 2024). These advantages make DC microgrids particularly attractive for applications such as electric vehicles, residential energy systems, data centres and smart buildings. A key component of DC microgrids is the DC–DC power converter, especially bidirectional topologies, which regulate the DC bus voltage and enable bidirectional power flow among energy storage units, renewable sources and load buses. Bidirectional converters provide voltage adaptation, controlled energy exchange and energy buffering capabilities, which are essential when storage systems must absorb excess generation or supply power during load transients (Dragičević et al., 2015; Tuluhong et al., 2025).

* Email: fatemeh.rezayof_tatari.dokt@pw.edu.pl

Despite their importance, achieving fast, robust and stable voltage regulation in bidirectional DC–DC converters remains challenging due to several inherent characteristics. Many converter topologies, particularly boost and bidirectional structures, exhibit non-minimum phase (NMP) behaviour during step-up operation. The presence of a right-half-plane (RHP) zero in their transfer function causes the output voltage to initially deviate in the opposite direction of the applied control action, thereby limiting the achievable control bandwidth (Li et al., 2023; Padhee and Murari, 2022). Excessively aggressive control actions may result in large inductor-current ripple, voltage overshoot, or closed-loop instability. Moreover, bidirectional operation over wide input–output ranges introduces strong non-linear and time-varying dynamics that further degrade the performance of classical linear controllers (Li et al., 2023).

These challenges are further exacerbated by the widespread presence of constant-power loads (CPLs) in modern DC systems. Power-electronic interfaces and tightly regulated converters often behave as CPLs (Effah et al., 2024), drawing nearly constant power regardless of bus voltage variations. This behaviour introduces negative incremental impedance, which reduces system damping and may destabilise the system at both converter and network levels (Abdurraqeeb et al., 2024). The combined effects of NMP dynamics, non-linearities and CPL-induced negative impedance significantly complicate voltage regulation and motivate the use of advanced control strategies.

A wide range of control approaches has been proposed to solve these issues (Forouzesh et al., 2017). Proportional–integral (PI) controllers (Guo et al., 2023) are widely adopted due to their simplicity and ease of implementation; however, their performance deteriorates under non-linear dynamics, bidirectional power flow, large disturbances and CPL-driven instabilities. Current-mode hysteresis and bang-bang (BB) controllers provide fast transient response and inherent current limiting but suffer from variable switching frequency, increased ripple and sensitivity to measurement noise and digital implementation delays (Lopez-Santos et al., 2021). Non-linear control methods, including sliding-mode (Shtessel et al., 2014), passivity-based (Michel et al., 2023) and backstepping control (Wu and Lu, 2019), improve robustness under non-linear and CPL conditions but typically require accurate system models and may introduce chattering or increased design complexity.

Given that power converters inherently operate in a finite number of discrete switching states, control strategies that directly exploit this intrinsic discrete nature have attracted increasing attention. Finite-state control paradigms—including finite-set model predictive control (FS-MPC) and BB–based approaches—operate directly on admissible switching states, enabling fast dynamic response and low computational overhead while avoiding intermediate modulation stages.

Model predictive control (MPC) (Nduwamungu et al., 2024) has also emerged as an effective control strategy for power converters operating under non-linear dynamics and system constraints. In continuous-set MPC (CS-MPC), the control action is obtained by solving a continuous optimisation problem to compute an optimal duty cycle, whereas FS-MPC directly evaluates a discrete set of admissible switching states, making it particularly suitable for digitally controlled power converters. Compared with CS-MPC, FS-MPC provides faster dynamic response and improved disturbance rejection; however, conventional single-horizon FS-MPC faces challenges in regulating the output voltage of NMP converters, as the short prediction horizon is insufficient to compensate for the inherent inverse response. Although extending the prediction horizon can alleviate this limitation, it significantly increases computational complexity, thereby constraining real-time implementation on embedded platforms (Tatari et al., 2024).

Strategies such as move blocking have been proposed to reduce the number of optimisation variables, which will reduce computational demand (Tatari et al., 2023, 2024); nevertheless, these approaches still require high-performance processing hardware for real-time operation. Alternatively, enhanced single-horizon MPC schemes (Tatari et al., 2025) have been developed for boost converters in which inductor-current regulation is incorporated into the cost function. By simultaneously enforcing voltage and current control objectives, these methods effectively mitigate NMP behaviour without any need for a long prediction horizon. Despite their advantages, most of these approaches rely on direct load-current measurement, which increases hardware cost and sensitivity to noise. A load-current estimation-based MPC technique has been introduced in Tatari et al. (2025) to reduce sensor requirements while maintaining robustness under varying load conditions; however, these methods remain model-dependent, and their performance is inherently sensitive to parameter uncertainties and modelling errors.

Moreover, fast-switching strategies—particularly conventional BB control (Barreto et al., 2004)—remain attractive due to their structural simplicity and negligible computational cost. However, the discrete nature of digital implementation inherently introduces a one-sample computational delay between state measurement and

switching action. This delay reduces the precision of current regulation, leading to increased inductor-current ripple and, consequently, a degradation in voltage-regulation performance (Buso and Mattavelli, 2022). To address this issue, compensated BB (CMP-BB) control schemes are used, which employ a mathematical model of the system to update the state variables by one step to compensate for the one-sample delay introduced by digital implementation. This state-update mechanism improves the accuracy of the switching decision and mitigates the adverse effects of the digital delay, while preserving the inherent simplicity and fast response of BB switching. When combined with load-current estimation, such an approach can achieve dynamic performance comparable to short-horizon FS-MPC, yet with significantly lower computational effort. Nevertheless, since the delay compensation relies on the accuracy of the system model, the control performance remains sensitive to parameter uncertainties, and steady-state voltage errors may arise if the desired inductor-current reference is not properly determined.

As an alternative control strategy intended to reduce model dependence and computational complexity, BB control can be implemented at a doubled sampling frequency (DSF-BB), yielding performance comparable to the two previously discussed strategies, with only negligible differences. Under this configuration, satisfactory dynamic performance can be achieved even without explicit compensation of the one-sample digital delay. Nevertheless, load-current estimation remains necessary to compute the desired inductor-current reference employed in the control law to ensure proper voltage regulation. If this reference is omitted, the intrinsic voltage–current coupling of boost-type converters cannot be adequately compensated, resulting in steady-state voltage deviation. Although this approach exhibits lower computational burden and reduced reliance on the system model compared to fully model-based strategies, it still requires load-current estimation and therefore retains a limited degree of model dependence.

To eliminate dependence on the system model, a model-free bang-bang (MF-BB) control strategy is adopted in this work. In this approach, the control formulation does not require explicit knowledge of the converter dynamics, thereby removing the need for model-based state updates or prediction. Despite this simplification, the proposed strategy achieves transient and steady-state performance comparable to that of the model-based approaches, while operating independently of model accuracy. Moreover, an alternative formulation of the desired inductor-current reference is introduced that does not rely on load-current information. Consequently, the proposed MF-BB strategy eliminates the need for load-current estimation and model-based prediction, significantly reducing sensitivity to parameter uncertainty and modelling errors. The details of the proposed MF-BB control strategy and its underlying principles are presented in the following sections.

Motivated by these trade-offs, this paper presents a systematic comparison of recent advanced control strategies for bidirectional DC–DC converters. The investigated methods include:

- single-horizon FS-MPC with load-current estimation reported in Tatari et al. (2025),
- CMP-BB control with digital-delay compensation and load-current estimation,
- BB control implemented at double sampling frequency, DSF-BB, using estimated current and
- a newly proposed MF-BB control strategy.

The controllers are compared in terms of dynamic response, steady-state accuracy, robustness and implementation complexity. Their performance is evaluated under realistic operating conditions, including NMP behaviour, parameter variations and digital control delays. Additionally, robustness is examined under varying system inertia by applying large variations in output capacitance, which represent changes in energy-storage characteristics. Both comprehensive simulation and experimental results are provided to validate the comparative analysis and demonstrate the practical applicability of the investigated control strategies.

2. System Description

2.1. Bidirectional converter topology

Figure 1 illustrates the bidirectional DC–DC converter considered in this study. The converter comprises an inductor L, an output capacitor C and two complementary switch–diode pairs S_1, D_1 and S_2, D_2, forming the lower and upper legs of the converter. The input and output voltages are denoted by u_s and u_{out}, respectively. The inductor current, capacitor current and load current are represented by i_L, i_C, and i_{Load}, respectively.

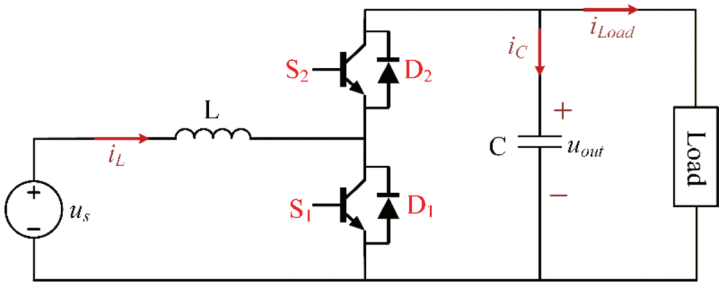

Figure 1. Bidirectional converter schematic.

The inductor current direction uniquely determines the direction of power flow. A positive inductor current indicates energy transfer from the input source to the DC bus, and a negative inductor current indicates energy transfer from the DC bus back to the source.

Table 1 also summarises the system parameters used in the simulation studies presented in this work.

Table 1. System parameters.

Parameters	Symbols	Values
Input voltage	u_s	100V
Output desired voltage	u_{ref}	160–240V
Maximum and minimum inductor current values	i_L^{max}, i_L^{min}	±20 A
Resistive load changes	R	50 Ω–1 kΩ
Input inductance	L	750 μH
Output capacitance	C	200–1500 μF
Sampling time	T_s	20 μs
Weighting factor	ω_i	1.0–0.2

Model-based control techniques, particularly MPC-based approaches, require an accurate mathematical representation of the converter dynamics to predict future behaviour and compute appropriate switching actions. Therefore, the continuous- and discrete-time models of the bidirectional converter are derived in the following subsections.

2.2. Continuous-time converter model

The inductor current is defined as positive when it flows from the input source towards the DC bus. Negative values of i_L indicate power transfer from the DC bus back to the source. The load current i_{Load} is defined as positive when drawn from the DC bus by the load. The input voltage is assumed to be stiff, and the converter regulates the output voltage. The dynamic behaviour of the bidirectional DC–DC converter can be described using a unified continuous-time model. The governing equations remain valid for both directions of power flow, with the sign of the inductor current determining the direction of energy transfer.

2.2.1. Mode 1: Inductor energy accumulation

During this interval, the inductor is energised, and the magnitude of the inductor current increases. Energy is transferred into the inductor either from the input source or from the DC bus, depending on the operating condition. During this interval, the output capacitor supplies the load current.

The corresponding system dynamics are given by

$$\frac{di_L(t)}{dt} = \frac{1}{L} u_s(t) \tag{1}$$

$$\frac{du_{out}(t)}{dt} = -\frac{1}{C} i_{Load}(t) \tag{2}$$

2.2.2. Mode 2: Inductor energy release

In the complementary interval, the energy stored in the inductor is released. Depending on the operating point, this energy is transferred either to the DC bus or back to the input source. During this interval, the inductor contributes to the supplying load and charging or discharging the output capacitor. The system dynamics in this interval are described by

$$\frac{di_L(t)}{dt} = \frac{1}{L}\left(u_s(t) - u_{out}(t)\right) \tag{3}$$

$$\frac{du_{out}(t)}{dt} = \frac{1}{C}\left(i_L(t) - i_{Load}(t)\right) \tag{4}$$

The above equations provide a unified description of the converter dynamics that is valid for both directions of power flow. The instantaneous direction of energy transfer is determined by the sign of the inductor current and by the relative magnitudes of the input and output voltages, rather than by distinct circuit configurations.

When the converter regulates the output voltage under step-up operating conditions, the system exhibits NMP behaviour due to the inherent RHP zero associated with boost-type energy transfer. This characteristic fundamentally limits the achievable voltage-control bandwidth and motivates the use of advanced control strategies. During reverse power-flow operation, the dynamic behaviour differs; however, the same state equations remain applicable.

2.3. Discrete-time model for MPC implementation

For finite state control strategies that directly compute switching actions—such as FS-MPC and BB control—the continuous-time converter model must be expressed in discrete-time form. This requirement arises because switching decisions are updated at discrete sampling instants, and digital implementation inherently introduces a one-sample delay between state measurement and actuation. Properly accounting for this delay is essential to ensure accurate state evaluation and stable closed-loop operation.

In this study, the continuous-time model is discretised using the forward Euler method with a sampling period T_s. The selected sampling period is sufficiently smaller than the dominant electrical time constants of the converter, ensuring that the forward Euler discretisation accurately captures the system dynamics within the control bandwidth. Application of this discretisation to the converter dynamics yields the following discrete-time state equations.

2.3.1. Mode 1: Storing energy in inductor

$$i_L(k+1) = \frac{T_s}{L}u_s(k) + i_L(k) \tag{5}$$

$$u_{out}(k+1) = \frac{-T_s}{C}i_{Load}(k) + u_{out}(k) \tag{6}$$

2.3.2. Mode 2: Releasing energy from inductor

$$i_L(k+1) = \frac{T_s}{L}\left(u_s(k) - u_{out}(k)\right) + i_L(k) \tag{7}$$

$$u_{out}(k+1) = \frac{T_s}{C}\left(i_L(k) - i_{Load}(k)\right) + u_{out}(k) \tag{8}$$

These discrete-time equations describe the sampled evolution of the inductor current and output voltage and form the basis for the state-update and delay-compensation mechanisms employed by the model-based control strategies discussed in the following section.

3. Model-Based Control Strategies

As mentioned, model-based control strategies rely on an explicit mathematical representation of the converter dynamics to update or predict future system behaviour and determine appropriate switching actions. By embedding the system model within the control law, these methods can compensate for digital implementation delays, account for system constraints and enhance regulation performance under non-linear operating conditions.

3.1. Finite set model predictive control

The discrete-time model derived in Section 2.3 is employed within a single-horizon FS-MPC framework to determine the optimal switching action while compensating for the one-sample digital delay inherent to digital implementation. At each sampling instant, the measured state variables are first updated using the discrete-time model to obtain the states at $k + 1$, thereby compensating for the one-sample delay inherent to digital control. Subsequently, a one-step-ahead prediction is performed from the updated states to estimate the system variables at $k + 2$ for each admissible switching action, and the corresponding predicted values are used to support the switching decision.

$$i_{pred} = i_L(k+2) = \frac{T_s}{L}\left(u_s(k+1) - \left(1 - s(k+1)\right)u_{out}(k+1)\right) + i_L(k+1) \tag{9}$$

$$u_{pred} = u_{out}(k+2) = \frac{T_s}{C}\left(\left(1 - s(k+1)\right)i_L(k+1) - i_{Load}(k+1)\right) + u_{out}(k+1) \tag{10}$$

In Eqs (9) and (10), the state variables at $k + 1$ represent the delay-compensated updated states, while the predicted values at $k + 2$ are employed to evaluate the candidate switching actions within the FS-MPC framework.

In the single-horizon FS-MPC formulation reported in Tatari et al. (2025), the control action is selected by evaluating two cost functions corresponding to the OFF ($s = 0$) and ON ($s = 1$) switching states. The switching state that minimises the cost function is applied to the converter. The corresponding cost functions are defined as

$$Err_0 = \left(u_{ref} - u^0_{pred}\right) + w_i\left(i_{des} - i^0_{pred}\right)^2 \tag{11}$$

$$Err_1 = -\left(u_{ref} - u^1_{pred}\right) + w_i\left(i_{des} - i^1_{pred}\right)^2 \tag{12}$$

In this formulation, i_{des} denotes the desired inductor-current reference introduced to ensure steady-state voltage regulation and overall system stability, while u^0_{pred}/i^0_{pred} and u^1_{pred}/i^1_{pred} represent the predicted output voltage/inductor current values at $k + 2$ corresponding to the OFF and ON switching states, respectively ($s = 0$ and $s = 1$ in Eqs (9) and (10)). The weighting factor w_i determines the trade-off between output-voltage tracking accuracy and inductor-current regulation and plays a critical role in achieving stable steady-state operation. The voltage-tracking errors are evaluated using the predicted output-voltage values; consequently, both the output voltage and the inductor current are assessed using predicted quantities in this FS-MPC formulation. The asymmetric voltage-error formulation in Eqs (11) and (12) is adopted to compensate for the converter's NMP behaviour exhibited during step-up operation. The negative sign in Err_1 accounts for the inverse initial response of the output voltage associated with the RHP zero, thereby enabling correct switching decisions within the FS-MPC framework.

Two cost functions in Eqs (11) and (12) can be unified into a single expression. Furthermore, the quadratic current-error term is replaced by its absolute value. In addition, instead of using the predicted output voltage u_{pred}, this paper adopts the measured output voltage $u_{out,act}$ for the evaluation of the voltage-tracking error. This choice is motivated by the fact that the output voltage is filtered by a relatively large capacitance, resulting in limited variation over consecutive sampling intervals. As demonstrated, this substitution does not affect switching decisions or closed-loop performance. On the contrary, this formulation yields regulation characteristics equivalent to those obtained using predicted voltage, while significantly reducing computational complexity and reliance on the converter model's accuracy. In contrast, the inductor current exhibits fast dynamics and directly reflects the instantaneous energy transfer within the converter; therefore, its predicted value is retained in the cost function to

preserve accurate current regulation and ensure correct switching decisions. Accordingly, the unified cost function used in this paper is expressed as

$$Err = (1-2s)\left(u_{ref} - u_{out,act}\right) + w_i \left| i_{des} - i_{pred} \right| \tag{13}$$

Inductor- Current Limitation: It should be noted that, in all control strategies investigated in this paper, an explicit control limit on the inductor current is implemented to ensure proper converter operation and prevent excessive current stress on the power components. The inductor current is constrained within predefined bounds

$$i_L^{min} \le i_L \le i_L^{max}$$

In the FS-MPC framework, this current limitation is enforced by saturating the predicted inductor current used in the cost-function evaluation. If a candidate switching state results in a predicted current exceeding the admissible bounds, the corresponding switching action is penalised and therefore avoided. This guarantees that the selected switching state maintains the inductor current within the acceptable operating region.

Load Current Estimation Technique: The desired inductor-current reference i_{des} is required to regulate the inductor current, limit current ripple and ensure accurate steady-state output-voltage regulation. This reference is derived using the principle of power balance. Assuming steady-state operation and neglecting converter power losses, which are small relative to the transferred power and therefore have a negligible impact on the power balance, the input and output powers can be approximated as equal, from which the desired inductor-current reference can be expressed as

$$P_{in} \simeq P_{out} \Rightarrow i_{des} = \frac{u_{ref}\, i_{Load}}{u_s} \tag{14}$$

where P_{in} and P_{out} represent the input and output power, respectively. Although direct measurement of the load current using an additional sensor is possible, it increases implementation cost and reduces system flexibility. To avoid this, a load-current estimation strategy reported in Tatari et al. (2025) is adopted in this work.

Using Kirchhoff's current law at the output node, the load current can be expressed as

$$i_{Load} = i_D - C\frac{u_{out}(k) - u_{out}(k-1)}{T_s} \tag{15}$$

In which, i_D denotes the diode current in the current sampling instant derived as

$$i_D = \left(1 - s(k-1)\right) i_L(k) \tag{16}$$

Here, k denotes the current sampling instant and $k - 1$ corresponds to the immediately preceding sampling instant. Substituting Eq. (16) into Eq. (15) yields an estimate of the load current. To improve estimation accuracy and reduce sensitivity to measurement noise, the average value of the inductor current over two consecutive sampling instants is employed, resulting in

$$i_{Load}^{est} = \left(1 - s(k-1)\right)\frac{i_L(k) + i_L(k-1)}{2} - C\frac{u_{out}(k) - u_{out}(k-1)}{T_s} \tag{17}$$

To further enhance robustness against measurement noise, the estimated load current is processed using a second-order low-pass filter with unity gain, a cutoff frequency of 200 Hz, and a damping ratio of $\xi = 1/\sqrt{2}$. This filtering stage improves estimation accuracy and ensures reliable operation under practical noisy sensing conditions.

Figure 2 illustrates the control scheme of the FS-MPC strategy reported in Tatari et al. (2025). At each sampling instant, the measured variables u_s, u_{out}, and i_L are first updated using Eqs (5)–(8) to compensate for the one-sample delay introduced by digital implementation, yielding the compensated states. Based on these values, a one-step-ahead prediction is performed using Eqs (9) and (10) to obtain $i_L(k + 2)$ and $u_{out}(k + 2)$. The predicted

variables, together with the desired inductor current i_L^{des} calculated from Eq. (14) using the estimated load current in Eq. (17) and a low-pass filter, are then used to evaluate the cost functions Eqs (11) and (12). The switching state that minimises the cost function is selected as $s(k + 1)$. An over-current protection mechanism is also enforced: if the compensated current $i_L(k + 1)$ exceeds the allowable limit i_L^{max}, the switch is disabled; otherwise, the selected switching state is applied. Finally, after a one-sample delay block, the switching command s is generated for the converter switches. It should be noted that the load-current estimation uses the previous switching state $s(k - 1)$, which introduces an effective two-sample delay in the control loop.

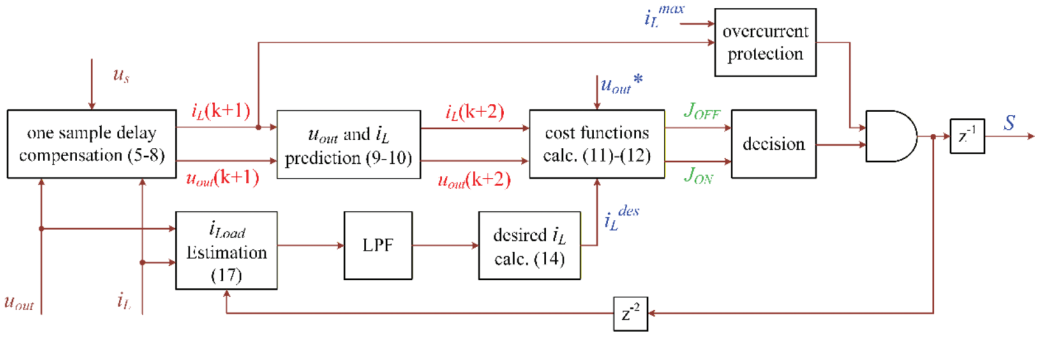

Figure 2. FS-MPC block diagram with prediction of both inductor current and output voltage (Tatari et al., 2025). FS-MPC, finite-set model predictive control (LPF stands for low pass filter).

Figure 3 illustrates the modified FS-MPC control scheme. As discussed earlier, the measured output voltage is directly used in the cost-function evaluation, while only the inductor current is compensated and predicted. This simplification eliminates the need for voltage-state updating, thus reducing the computational burden of the control algorithm.

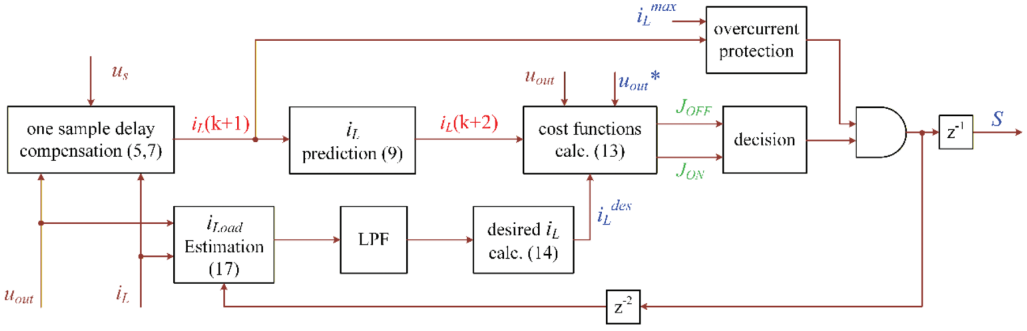

Figure 3. FS-MPC block diagram with inductor-current prediction and measured output voltage. FS-MPC, finite-set model predictive control.

The impact of using different voltage terms (predicted and actual values) in the FS-MPC cost function is illustrated in Figure 4, where formulations that use predicted and measured output voltages are compared. In both cases, accurate reference tracking is achieved for the output voltage and the inductor current. The transient responses exhibit comparable settling behaviour, with the output voltage settling to its steady-state value within approximately 20–30 ms following each operating-point change. Moreover, no noticeable steady-state voltage error is observed in either formulation.

As shown in Figure 4b, the inductor-current responses corresponding to the two voltage formulations are closely aligned, exhibiting nearly identical transient behaviour and ripple characteristics. These results indicate that replacing the predicted output voltage with the measured value does not adversely affect current regulation or voltage-tracking performance. Consequently, using measured output voltage in the FS-MPC cost function significantly reduces computational complexity and dependence on the system model without compromising control performance. Accordingly, in this paper, the measured output voltage is adopted for switching-state selection.

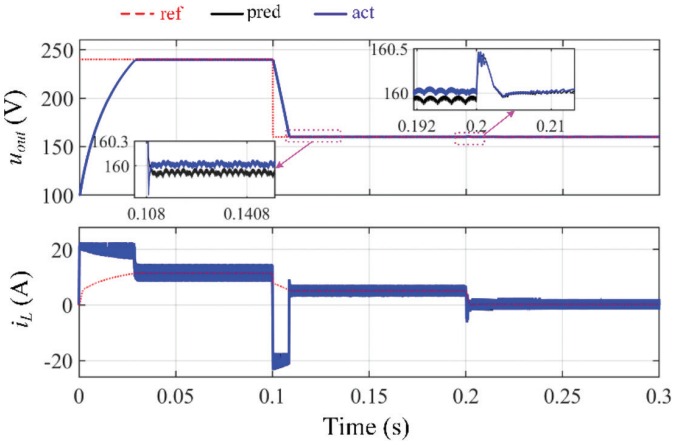

Figure 4. FS-MPC results with predicted and measured output voltage in the cost function: (a) output voltage, and (b) inductor current. FS-MPC, finite-set model predictive control.

3.2. CMP-BB method

In BB control schemes that rely on a system model, compensation of the one-sample digital delay can be achieved by updating the state variables by one sampling step, without requiring an additional prediction stage. As demonstrated in the previous section, only the inductor current requires one-sample state updating, whereas using the measured output voltage directly yields performance equivalent to that obtained with predicted or delay-compensated voltage values. It should be noted that, in BB control, the switching decision is determined directly by a switching function rather than by minimising an error-based cost function as in MPC. Consequently, the computational burden of BB control is significantly lower than that of MPC. Based on these considerations, the switching decision is formulated using the following switching function

$$S = \left(u_{ref} - u_{out,act}\right) + w_i \left| i_{des} - i_{comp} \right| \tag{18}$$

where i_{comp} denotes the delay-compensated inductor current used for the switching decision. It is obtained by updating the measured inductor current by one sampling step using the discrete-time model, and therefore corresponds to $i_L(k+1)$ as given by Eqs (5) and (7). Also, to maintain operation within admissible current limits and prevent excessive current stress on the power components, the same inductor-current limitation as described previously is also applied in this control strategy.

Figure 5 illustrates the block diagram and control sequence of the CMP-BB strategy. As shown, unlike the FS-MPC method, the switching state is determined directly through the switching function defined in Eq. (18). The delay-compensated inductor current $i_L(k+1)$, together with the measured output voltage and the desired current reference, are used to evaluate the switching function. The remaining blocks, including load-current estimation, filtering and over-current protection, operate in the same manner as described earlier.

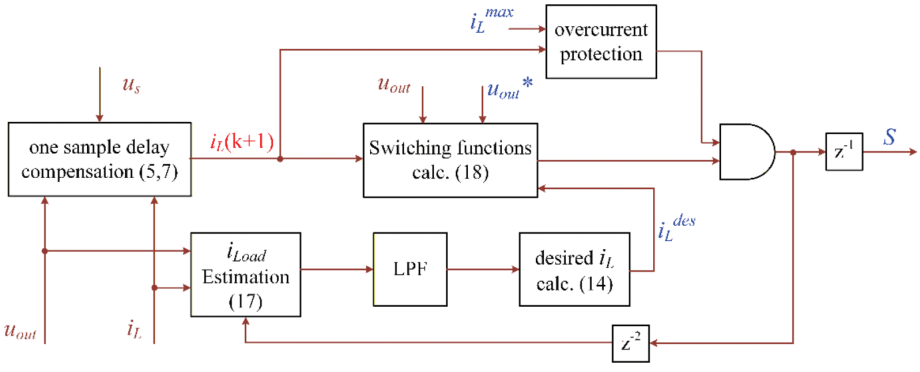

Figure 5. CMP-BB strategy block diagram with inductor-current compensation and measured output voltage. CMP-BB, compensated-BB.

Figure 6 presents the simulation results obtained using the CMP-BB control strategy for output-voltage regulation, including the output voltage, inductor current and load current. The reference output voltage is initially set to 240V and is stepped down to 160V at t = 0.1 s. To evaluate the controller performance under different conduction modes, the load resistance is varied from 50 Ω to 1 kΩ at t = 0.2 s after the system reaches steady-state, forcing a transition from continuous conduction mode (CCM) to discontinuous conduction mode (DCM).

As observed in Figure 6, the CMP-BB controller accurately tracks the reference voltage under both steady-state and transient operating conditions, including the transition from CCM to DCM. Following each voltage reference change, the output voltage settles to its steady-state value within approximately 20–30 ms, with no observable steady-state error. The inductor current remains well-regulated over the entire operating range and closely follows the desired current reference, exhibiting an acceptable ripple magnitude throughout the different operating modes. This behaviour confirms effective energy-transfer regulation during both transient and steady-state operation. Furthermore, the estimated load current closely aligns with the measured load current across all operating conditions, demonstrating the accuracy and effectiveness of the load-current estimation method. The close agreement between the estimated and measured load currents validates the suitability of the estimation approach for use within the control framework.

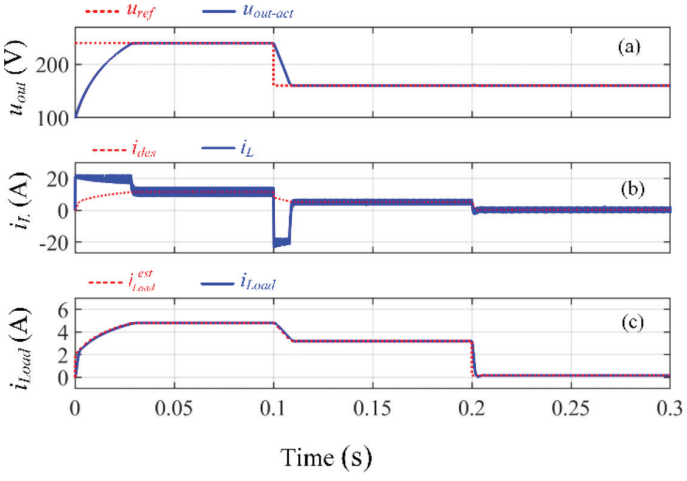

Figure 6. CMP-BB control results: (a) output voltage, (b) inductor current, and (c) load current. CMP-BB, compensated-BB.

3.3. Double sampling BB method

As discussed previously, to achieve performance comparable to FS-MPC and CMP-BB control while further reducing computational burden and dependence on the system model, BB control is implemented using a DSF-BB (i.e. f_s = 100 *k*Hz or T_s = 10 *μ*s, half the original sampling period). Under this configuration, the control algorithm is executed at a higher sampling rate, while the average switching frequency under identical operating conditions remains comparable to that of the standard sampling case. The increased sampling rate effectively mitigates the impact of the digital implementation delay, resulting in switching behaviour and inductor-current ripple comparable to those achieved with delay-CMP-BB control. Consequently, the double-sampling-frequency BB strategy achieves equivalent transient and steady-state performance without requiring model-based state updating.

Although the estimated load current is still employed to compute the desired inductor-current reference, the overall computational effort is significantly reduced as no predictive state update is required. This enables a simpler control structure with reduced reliance on the system model, while maintaining performance comparable to that of the previously discussed strategies.

The switching function used in this method is identical to that defined in Eq. (18), with the only difference being that the measured inductor current $i_{L,act}$ is used directly in place of the delay-compensated current i_{comp} for switching-state determination. As in the other control strategies, the inductor current is constrained within the previously defined admissible bounds to prevent overcurrent stress on the converter components.

The corresponding block diagram of the DSF-BB method is shown in Figure 7. The overall procedure is similar to the previous method; however, instead of compensating the digital delay through state updating, the controller

operates at a DSF-BB, which effectively mitigates the digital implementation delay and results in comparable control performance.

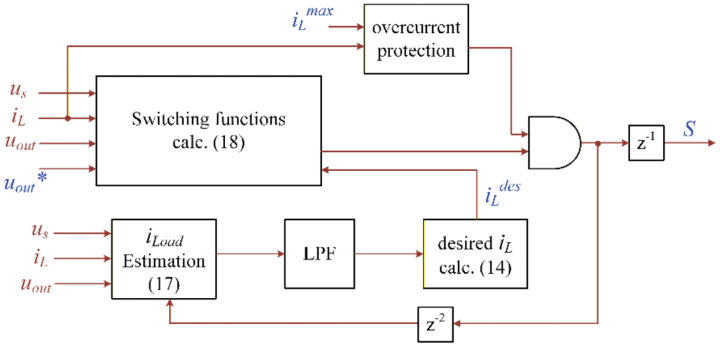

Figure 7. DSF-BB strategy block diagram with measured inductor-current and output voltage. DSF-BB, doubled sampling frequency.

Simulation results for the DSF-BB control method are presented in Figure 8 for the same operating scenarios considered previously. As shown, this strategy achieves effective output-voltage regulation with performance comparable to the previously discussed CMP-BB and FS-MPC strategies. Following each reference or operating-point change, the output voltage settles rapidly to its steady-state value, exhibiting no observable steady-state error. The settling behaviour is consistent with that observed in the preceding control strategies, indicating that the increased sampling rate effectively mitigates the impact of the digital implementation delay without requiring explicit model-based compensation.

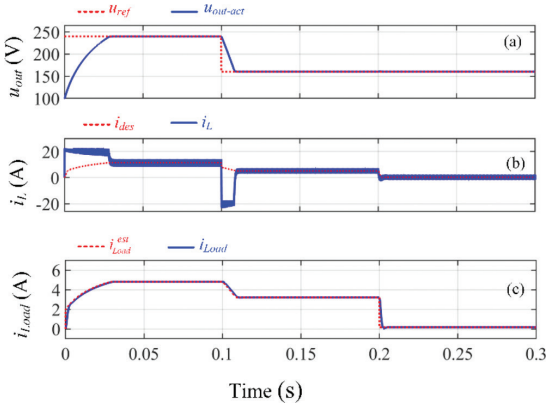

Figure 8. DSF-BB results: (a) output voltage, (b) inductor current and (c) load current. DSF-BB, doubled sampling frequency.

Moreover, the inductor current closely follows the desired current reference throughout the operating range, with a ripple magnitude comparable to that of the previous model-based approaches. This confirms that increasing the sampling frequency is sufficient to preserve accurate current regulation while maintaining a simple control structure. Overall, the current control and voltage regulation performance achieved with the DSF-BB is comparable to that of the two previously discussed strategies.

4. Proposed MF-BB Control

In the previous section, three variants of short-horizon control were implemented, and their corresponding results were presented. All three approaches exhibit some degree of dependence on the system model. Among them, FS-MPC relies most heavily on an accurate mathematical model, while the two BB-based strategies exhibit reduced, but still non-negligible, model dependence. In particular, even BB control implemented at a DSF-BB requires load-current information—estimated using model parameters—to compute the desired inductor-current reference.

Dependence on an accurate system model represents a practical limitation, since modelling errors, parameter variations and external disturbances are inevitable in real-world applications. These factors may degrade control performance and reduce robustness. To eliminate reliance on model-dependent information, a MF-BB control strategy is introduced in this paper.

The proposed MF-BB strategy is implemented at the same DSF-BB as the DSF-BB approach, i.e. 100 kHz, thereby preserving the short-horizon nature and fast dynamic response of the BB framework. Unlike the previously discussed strategies, the MF-BB approach does not rely on load-current information or an explicit converter model. Instead, the desired inductor-current reference is generated directly from the measured inductor current through a low-pass filtering process. This filtering operation suppresses switching-frequency ripple and attenuates high-frequency measurement noise, while preserving the low-frequency current dynamics required for accurate voltage regulation. As a result, the proposed approach enables fully model-free current-reference generation without sacrificing transient or steady-state performance.

The generation of the desired inductor-current reference is first defined in continuous time by the first-order low-pass transfer function as follows:

$$G_s = \frac{I_{des}(s)}{I_L(s)} = \frac{\omega_c}{s+\omega_c} \tag{19}$$

where $\omega_c = 2\pi f_c$ denotes the cutoff angular frequency of the filter. The cutoff frequency is selected as f_c = 321 Hz, which is sufficiently lower than the switching frequency to effectively attenuate switching-induced ripple while preserving the low-frequency current dynamics relevant for voltage regulation.

Since the control algorithm is implemented digitally, the continuous-time filter is discretised using the Tustin approximation, which provides a stability-preserving and symmetric mapping between the continuous- and discrete-time domains. Applying the Tustin transformation yields the following discrete-time recursive equation

$$i_{des}(k) = \alpha i_L(k) + \alpha i_L(k-1) + \beta\, i_{des}(k-1) \tag{20}$$

where the coefficients α and β are given by

$$\alpha = \frac{\frac{\omega_c T_s}{2}}{1+\frac{\omega_c T_s}{2}}$$

$$\beta = \frac{1-\frac{\omega_c T_s}{2}}{1+\frac{\omega_c T_s}{2}}$$

With a sampling period of T_s = 10 μs (f_s = 100 kHz) and the selected cutoff frequency f_c = 321 Hz, the resulting coefficients are $\alpha \approx 0.01$ and $\beta \approx 0.98$. Accordingly, the discrete-time filter is implemented as

$$i_{des}(k) = 0.01\, i_L(k) + 0.01\, i_L(k-1) + 0.98\, i_{des}(k-1) \tag{21}$$

where $i_L(k-1)$ and $i_{des}(k-1)$ denote the measured inductor current and the desired current reference at the previous sampling instant, respectively. The filter is executed at the same sampling rate as the control algorithm, ensuring synchronised operation and negligible additional computational burden. Owing to its recursive structure, the filtering scheme enables a fully model-free implementation while providing a smooth and well-behaved current reference.

Moreover, the MF-BB strategy employs the same switching function defined in Eq. (18), with the measured inductor current used directly for switching-state determination, consistent with the DSF-BB approach. As in the previously discussed strategies, identical inductor-current constraints are enforced to keep the operation within allowable current limits.

Figure 9 illustrates the block diagram of the proposed MF-BB control strategy. In contrast to the previous methods, this approach does not rely on the converter model or load-current estimation. Instead, the desired

inductor current is generated directly from the measured inductor current using the filtering relation defined in Eq. (21). The measured signals, together with the generated current reference, are then used in the switching function Eq. (18) to determine the switching state. As in the previous strategies, an over-current protection condition is applied to ensure safe operation.

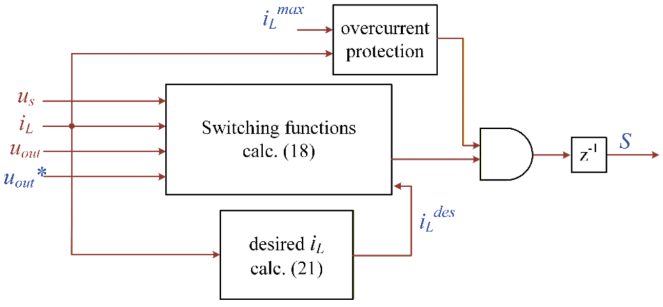

Figure 9. MF-BB strategy block diagram with measured inductor-current and output voltage. MF-BB, model-free bang-bang.

Simulation results for the proposed MF-BB strategy are presented in Figure 10. As shown in Figure 10a, the controller achieves accurate tracking of the reference output voltage under both transient and steady-state operating conditions. Following each reference change, the output voltage settles to its steady-state value within a time interval comparable to that of the previously discussed model-based strategies, with no observable steady-state voltage error. A small and practically negligible overshoot is observed during step-up transitions, together with a slight undershoot during step-down transitions. Considering that the proposed strategy completely eliminates reliance on an explicit system model, these minor transient deviations are negligible and do not detract from the overall regulation performance.

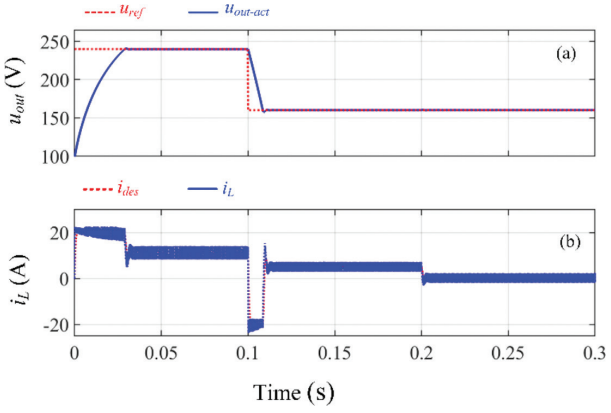

Figure 10. Model-free BB control results: (a) output voltage, and (b) inductor current. MF-BB, model-free bang-bang.

From the perspective of current regulation, Figure 10b indicates that the inductor current closely follows the desired current trajectory throughout the operating range, ensuring proper energy transfer and stable voltage regulation. Compared with the model-based strategies, the MF-BB controller exhibits a modest increase in instantaneous current ripple only during transient intervals; however, the steady-state ripple remains comparable across the strategies, and the ripple magnitude stays within acceptable limits without affecting the steady-state voltage performance.

5. Comparison Results

To evaluate the effectiveness of the proposed approach comprehensively, Figure 11 compares the MF-BB controller with the three previously discussed model-based strategies under identical operating conditions. As can be seen,

during the initial regulation to u_{ref} = 240 V, the MF-BB controller exhibits a small transient overshoot of approximately 0.7V (≈0.29% of 240V) before settling, which remains practically negligible. When the voltage reference is stepped down from 240V to 160V, a transient undershoot of approximately 2V (≈ 1.25%) is observed, as highlighted in the first zoomed region of Figure 11a. These deviations are consistent with the absence of model-based prediction and do not affect steady-state regulation.

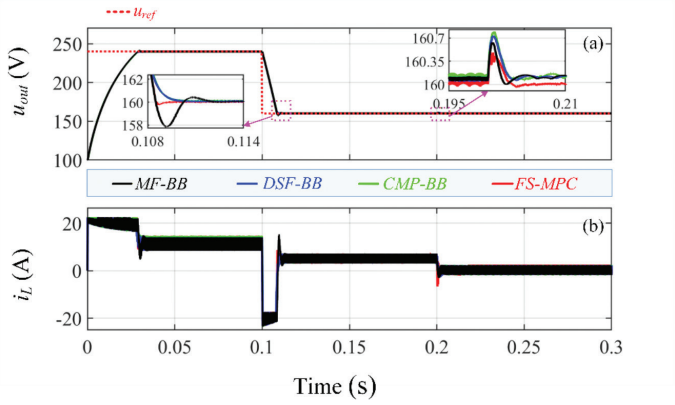

Figure 11. The comparison results for the three previous control methods and the proposed MF-BB considering: (a) output voltage, and (b) inductor current. MF-BB, model-free bang-bang.

More importantly, following the load change that forces operation into DCM, the second zoomed region in Figure 11a shows that the transient overshoot produced by the MF-BB controller is closely comparable to that of the model-based control strategies. This operating condition is particularly significant, as it directly evaluates the controller's capability to preserve voltage regulation and closed-loop stability in response to load disturbances, rather than commanded reference variations. Voltage regulation under load disturbances is practically a more relevant performance criterion in DC microgrid applications, as it reflects real operating conditions rather than idealised reference changes. In this post-disturbance stabilisation phase—highlighted by the second zoomed region—the proposed MF-BB strategy exhibits transient overshoot and settling characteristics that are closely comparable to those of the model-based control approaches. These observations indicate that, under practically relevant load changes, the proposed controller maintains robust voltage regulation and stable operation. Furthermore, the zoomed-in steady-state regions confirm that the MF-BB controller achieves precise tracking of the voltage reference with no significant steady-state error.

Figure 11b compares the inductor-current behaviour of the different control strategies. During transient intervals, the MF-BB controller exhibits a modest increase in instantaneous current ripple, which is a natural consequence of operating without model-based prediction or explicit delay compensation. In steady-state operation, the inductor-current ripple levels in all these control strategies are very similar. Overall, the observed differences in current ripple are subtle and practically negligible, and all controllers accurately regulate the average inductor current to the desired reference.

The results demonstrate that the proposed MF-BB control strategy achieves transient response, settling time and steady-state accuracy comparable to those of the three model-based control methods, while completely eliminating reliance on an explicit system model.

The proposed control strategy's performance is evaluated under reduced output-capacitance conditions, which correspond to operation with lower system inertia, to assess its robustness and practical applicability. In the previous simulations, the converter operated with a relatively large output capacitance of 1500 μF, representing a high-inertia DC bus with substantial energy-buffering capability. In this section, the output capacitance is reduced to 200 μF to investigate controller behaviour under faster system dynamics.

Reducing the output capacitance significantly increases the sensitivity of the DC-bus voltage to variations in the inductor current, which may lead to increased current ripple and more pronounced voltage deviations during transients. To account for these effects and ensure stable operation under low-inertia conditions, the weighting factor w_i in the switching and cost-function formulations is increased from w_i = 0.2 to w_i = 1.0 for all control strategies considered in this scenario. This adjustment places greater emphasis on inductor-current regulation, thereby limiting

current ripple while maintaining acceptable voltage-tracking performance. The selected value reflects a deliberate trade-off between voltage-error minimisation and current-regulation objectives, which becomes more critical as the system inertia decreases. Applying the same weighting factor across all strategies ensures a fair and consistent performance comparison.

Figure 12 represents the simulation results of the proposed MF-BB control strategy under low-inertia conditions. As shown in Figure 12a, the controller continues to track the output-voltage reference accurately despite the substantial reduction in capacitance. The output voltage remains stable for both reference and load changes, and no steady-state voltage error is observed. Figure 12b further shows that the inductor current remains well-regulated throughout the operating range, confirming that proper energy transfer is maintained even under faster system dynamics.

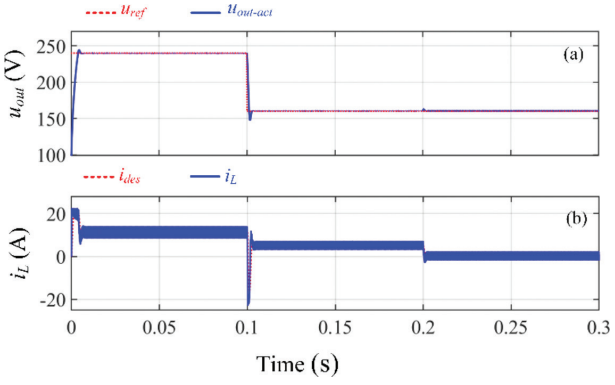

Figure 12. MF-BB control performance under low-inertia operation (C=200 μF): (a) output voltage, and (b) inductor current. MF-BB, model-free bang-bang.

As expected, the reduction in output capacitance results in a faster transient response due to the lower effective inertia of the system. Consequently, the settling time following voltage-reference changes and load disturbances is reduced compared to the high-capacitance case. This behaviour is consistent with the underlying physical dynamics of the converter and does not indicate degradation of the control performance. Rather, it demonstrates the ability of the proposed strategy to adapt to significantly altered system dynamics while preserving stability and regulation accuracy.

Figure 13 also compares the performance of all control strategies examined in this paper under the same low-capacitance condition. Due to the reduced energy-storage capability of the DC bus, an increase in output-voltage ripple is observed for all strategies, which is an expected consequence of operating with a smaller output capacitor. Quantitatively, the voltage ripple increases from approximately 0.05% in the high-inertia case (1500 µF) to about 0.4% under low-inertia operation (200 µF). This increase is a direct consequence of the reduced energy-storage capability of the DC bus and does not indicate a limitation of the proposed control strategy. Nevertheless, all control strategies maintain stable operation, and no oscillatory or unstable behaviour is observed.

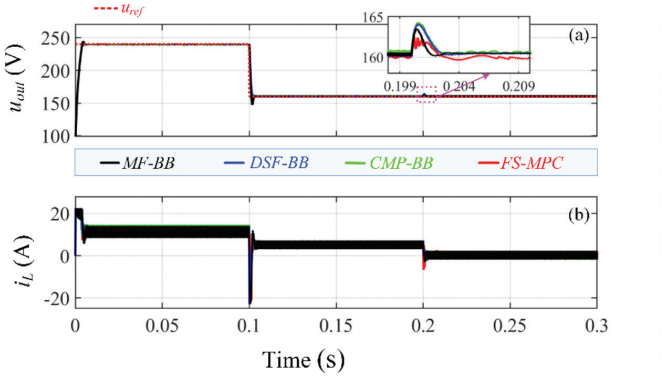

Figure 13. The comparison results for the three previous control methods and the proposed MF-BB under low-inertia operation (C=200 μF): (a) output voltage, and (b) inductor current. CMP-BB, compensated-BB; DSF-BB, doubled sampling frequency; FS-MPC, finite-set model predictive control; MF-BB, model-free bang-bang.

The zoomed-in regions in Figure 13a further indicate that the proposed MF-BB strategy not only preserves closed-loop stability under reduced inertia but also achieves a settling response comparable to, and in some cases faster than, those of the model-based strategies following load disturbances. Overall, these results confirm that the proposed MF-BB control strategy remains effective and robust under significant variations in system inertia, thereby validating its suitability for practical DC microgrid applications in which output capacitance and system dynamics may vary considerably.

6. Experimental Results

In this section, experimental results are presented to validate the simulation findings and to demonstrate the practical feasibility of the proposed control strategy. The experimental setup is configured according to the system parameters listed in Table 1, with minor adjustments imposed by hardware limitations. Specifically, the inductor current is constrained within ±10 A. Moreover, the resistive load is set to 100 Ω under steady-state conditions, while during transient tests, it is varied between 50 Ω and 100 Ω to evaluate system performance under load disturbances.

The experimental investigation includes both steady-state and transient operating conditions to assess the effectiveness of the proposed MF-BB controller comprehensively.

Under steady-state operation, the system performance is evaluated at different reference voltages. Figure 14 illustrates the steady-state waveforms of the output voltage for reference values of 150V, 200V and 240V. As observed, the proposed control strategy maintains the output voltage at the desired reference levels across all operating points, with stable operation and consistent regulation behaviour.

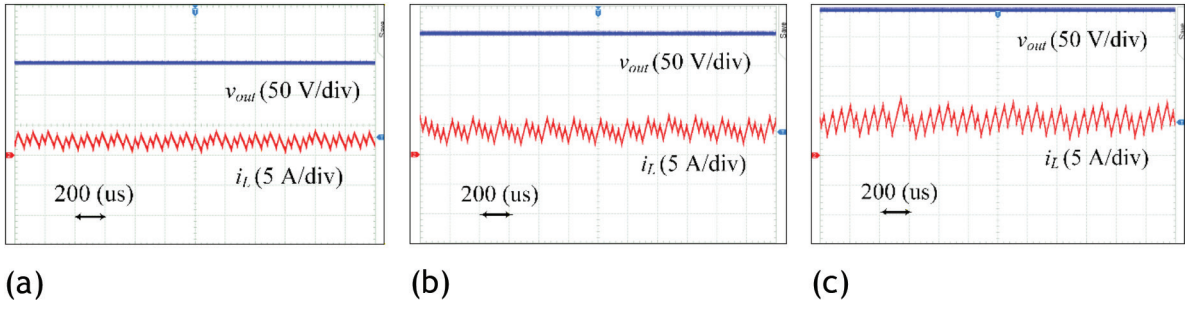

Figure 14. Steady-state output-voltage waveforms of the bidirectional converter under a 100 Ω resistive load for different reference voltages: (a) 150V, (b) 200V, and (c) 240V.

To further assess the dynamic performance, transient tests are conducted under step changes in the reference voltage. In this scenario, the reference voltage is varied from 160V to 240V (step-up) and from 240V to 160V (step-down). The corresponding results are presented in Figure 15, which shows that the controller has a fast dynamic response, with the output voltage closely following the reference transitions. The system exhibits smooth transient behaviour with limited overshoot and undershoot and the voltage rapidly settles to its steady-state value.

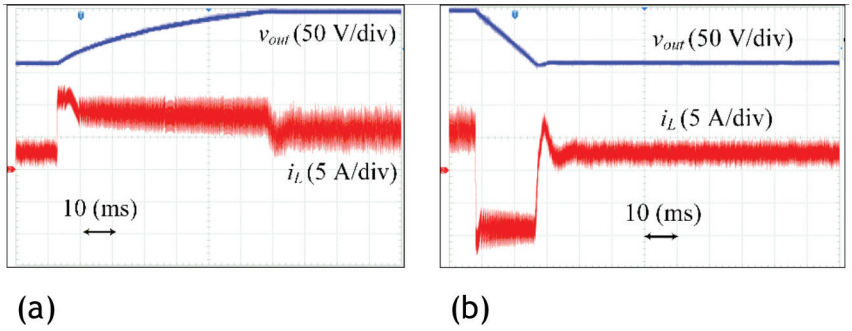

Figure 15. Dynamic response of the bidirectional converter using the proposed control strategy under reference voltage transitions with a 100 Ω resistive load: (a) step-up from 160V to 240V, and (b) step-down from 240V to 160V.

In addition, the robustness of the proposed control strategy is evaluated under load disturbances. In this case, the resistive load is varied from 100 Ω to 50 Ω and vice versa, while maintaining a constant reference voltage of 200V. The corresponding results are presented in Figure 16. Following each load change, the output voltage exhibits only a slight, but practically insignificant variation, as highlighted in the zoomed-in region. This minor fluctuation is rapidly suppressed, and the voltage quickly returns to its reference value, indicating effective disturbance rejection.

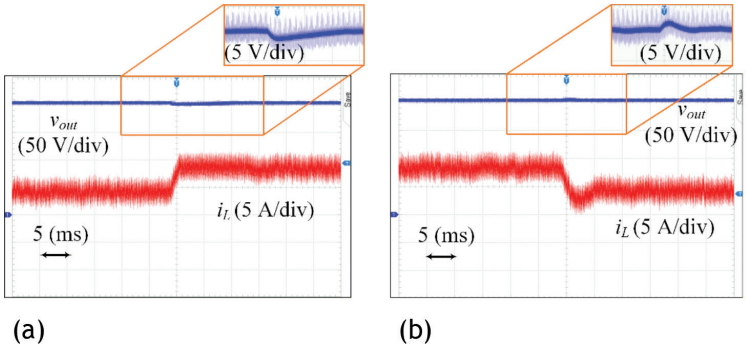

Figure 16. Dynamic response of the bidirectional converter using the proposed control strategy under load variations at a reference voltage of 200V: (a) load change from 100 Ω to 50 Ω, and (b) load change from 50 Ω to 100 Ω

7. Conclusion

This paper presented a systematic comparison of short-horizon finite-state control strategies for output-voltage regulation of a bidirectional DC–DC converter operating under NMP dynamics. Four approaches were investigated: single-horizon FS-MPC, CMP-BB control with digital-delay compensation, BB control implemented at a DSF-BB and a newly proposed MF-BB strategy. A unified continuous- and discrete-time converter model was derived to ensure consistent controller formulation and fair comparison. Based on this framework, the corresponding cost functions and switching laws were developed and the controllers were evaluated through comprehensive simulation studies under realistic operating conditions, including voltage-reference changes, load disturbances, CCM–DCM transitions and variations in system inertia.

The results demonstrate that the model-based strategies provide fast transient response and accurate steady-state voltage regulation when accurate system models and reliable load-current estimation are available. But their performance remains dependent on model fidelity and parameter knowledge. In contrast, the proposed MF-BB strategy completely removes reliance on an explicit system model while achieving transient response, settling time and steady-state accuracy comparable to the model-based approaches. Robustness analysis under reduced system inertia further confirms stable operation and effective voltage regulation despite increased voltage ripple and faster dynamics. Both simulation and experimental results validate these findings and confirm the practical applicability of the proposed control approach. In conclusion, the MF-BB control strategy offers a computationally efficient, robust and model-independent solution for short-horizon finite-state voltage control of bidirectional DC–DC converters with NMP behaviour, making it a suitable choice for practical real-time implementation in DC microgrids and energy storage applications.

Acknowledgement

This research was funded by the National Science Centre, Poland [grant number PRELUDIUM - 2025/57/N/ST7/01859].

References

Abdurraqeeb, A. M., Al-Shamma'a, A. A., Alkuhayli, A., Alharbi, M., Farh, H. M. H., Alsaif, F., Omotoso, H. O., Addoweesh, K. E. and Qamar, A. (2024). Stabilization of Constant Power Loads and Dynamic Current Sharing in DC Microgrid Using Robust Control Technique. *Electric Power Systems Research*, 230, p. 110258. doi: 10.1016/j.epsr.2024.110258

Al-Ismail, F. S. (2021). DC Microgrid Planning, Operation, and Control: A Comprehensive Review. *IEEE Access*, 9, pp. 36154–36172. doi: 10.1109/ACCESS.2021.3062840

Barreto, L. H. S. C., Coelho, E. A. A., Farias, V. J., de Freitas, L. C. and Vieira, J. J. B. (2004). The Bang-Bang Hysteresis Current Waveshaping Control Technique Used to Implement a High Power Factor Power Supply. *IEEE Transactions on Power Electronics*, 19(1), pp. 160–168. doi: 10.1109/TPEL.2003.820591

Bizhani, H., Iwański, G. and Noroozian, R. (2025). Renewable Energy Conversion and Energy Storage Systems—Summary of the Special Section. *Power Electronics and Drives*, 10, pp. 508–511. doi: 10.2478/pead-2025-0032

Buso, S. and Mattavelli, P. (2022). *Digital Control in Power Electronics*. Springer Nature, Cham, Switzerland.

Dragičević, T., Lu, X., Vasquez, J. C. and Guerrero, J. M. (2015). DC Microgrids—Part I: A Review of Control Strategies and Stabilization Techniques. *IEEE Transactions on Power Electronics*, 31(7), pp. 4876–4891, July 2016, doi: 10.1109/TPEL.2015.2478859.

Effah, E. K., Anto, E. K., Okyere, P. Y. and Effah, F. B. (2024). Model Reference Adaptive Control of SPS-Based Dual Active Bridge Converter with Constant Power Loading. *Power Electronics and Drives*, 9(1), pp. 348–357. doi: 10.2478/pead-2024-0022

Forouzesh, M., Siwakoti, Y. P., Gorji, S. A., Blaabjerg, F. and Lehman, B. (2017). Step-Up DC–DC Converters: A Comprehensive Review of Voltage-Boosting Techniques, Topologies, and Applications. *IEEE Transactions on Power Electronics*, 32(12), pp. 9143–9178. doi: 10.1109/TPEL.2017.2652318

Guo, Q., Bahri, I., Diallo, D. and Berthelot, E. (2023). Model Predictive Control and Linear Control of DC–DC Boost Converter in Low Voltage DC Microgrid: An Experimental Comparative Study. *Control Engineering Practice*, 131, p. 105387. doi: 10.1016/j.conengprac.2022.105387

Li, Y., Sahoo, S., Dragičević, T., Zhang, Y. and Blaabjerg, F. (2023). Stability-Oriented Design of Model Predictive Control for DC/DC Boost Converter. *IEEE Transactions on Industrial Electronics*, 71(1), pp. 922–932. doi: 10.1109/TIE.2023.3247785

Lopez-Santos, O., Dantonio, D. S., Flores-Bahamonde, F. and Torres-Pinzón, C. A. (2021). Hysteresis control methods. In: *Multilevel Inverters*. Academic Press, pp. 35–60.

Michel, Y., Saveriano, M. and Lee, D. (2023). A Passivity-Based Approach for Variable Stiffness Control With Dynamical Systems. *IEEE Transactions on Automation Science and Engineering*, 21(4), pp. 6265–6276. doi: 10.1109/TASE.2023.3324141

Nduwamungu, A., Lie, T. T., Lestas, I., Nair, N. K. C. and Gunawardane, K. (2024). Control Strategies and Stabilization Techniques for DC/DC Converters Application in DC MGs: Challenges, Opportunities, and Prospects—A Review. *Energies*, 17(3), p. 669. doi: 10.3390/en17030669

Padhee, S. and Murari, R. (2022). Study the effect of right-half plane zero on voltage-mode controller design for boost converter. In: *Control Applications in Modern Power Systems: Select Proceedings of EPREC 2021*. edited by Jitendra Kumar, Manoj Tripathy, and Premalata Jena, Singapore: Springer Nature Singapore, pp. 95–106.

Patel, V., Giri, V. K. and Kumar, A. (2024). Efficient Power Management Strategies for AC/DC Microgrids With Multiple Voltage Buses for Sustainable Renewable Energy Integration. *Energy Informatics*, 7(1), p. 97. doi: 10.1186/s42162-024-00377-5

Shtessel, Y., Edwards, C., Fridman, L. and Levant, A. (2014). *Sliding Mode Control and Observation*. vol. 10. New York: Springer New York.

Tatari, F. R., Banejad, M. and Kalat, A. A. (2023). A Move Blocking Based Direct Voltage Model Predictive Control to Enhance The Dynamic Performance of DC Microgrids Containing Constant Power Loads. *IET Renewable Power Generation*, 17(13), pp. 3340–3354. doi: 10.1049/rpg2.12848

Tatari, F. R., Banejad, M., Kalat, A. A. and Iwanski, G. (2024). A Long-Horizon Move-Blocking Based Direct Power Model Predictive Control for Dynamic Enhancement of DC MICROGRIDs. *Ain Shams Engineering Journal*, 15(7), p. 102837. doi: 10.1016/j.asej.2024.102837

Tatari, F. R., Bizhani, H. and Iwanski, G. (2025). Split Cost Function Based Single-Horizon Finite-Set Model Predictive Control for Boost Converter with Loading Current Estimation. *IEEE Journal of Emerging and Selected Topics in Power Electronics*, vol. 13, no. 4, pp. 5071-5083, Aug. 2025, doi: 10.1109/JESTPE.2025.3535101.

Tuluhong, A., Xu, Z., Chang, Q. and Song, T. (2025). Recent Developments in Bidirectional DC-DC Converter Topologies, Control Strategies, and Applications in Photovoltaic Power Generation Systems: A Comparative Review and Analysis. *Electronics*, 14(2), p. 389. doi: 10.3390/electronics14020389

Wu, J. and Lu, Y. (2019). Adaptive Backstepping Sliding Mode Control for Boost Converter With Constant Power Load. *IEEE Access*, 7, pp. 50797–50807. doi: 10.1109/ACCESS.2019.2910936